Check for updates

View Article Online
View Journal

NORGANIC CHEMISTRY

FRONTIERS

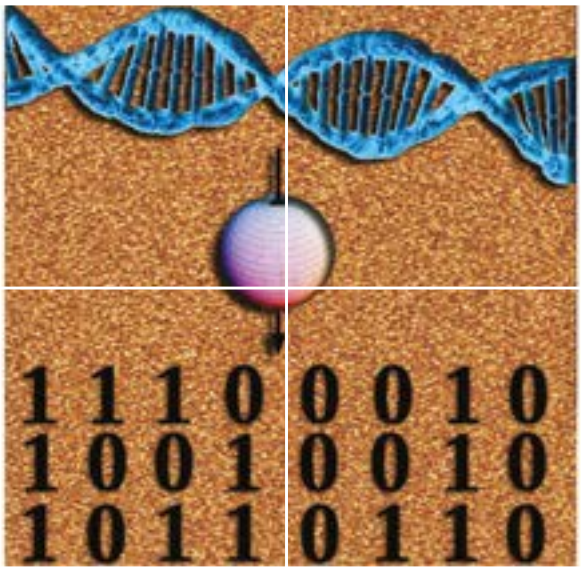

ccepted Manuscript

This article can be cited before page numbers have been issued, to do this please use: M. KOTZABASAKI and G. Froudakis, *Inorg. Chem. Front.*, 2018, DOI: 10.1039/C7QI00645D.

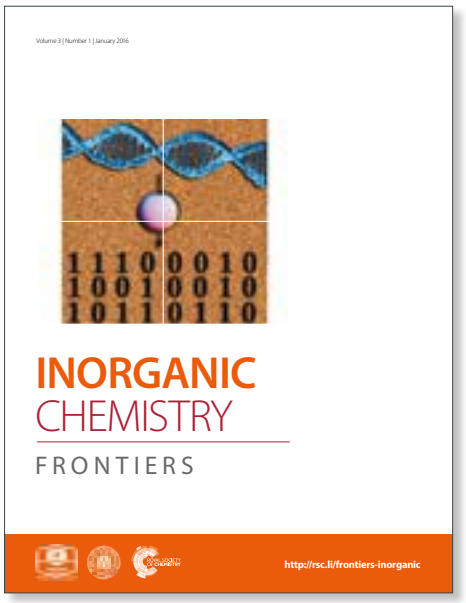

This is an Accepted Manuscript, which has been through the Royal Society of Chemistry peer review process and has been accepted for publication.

Accepted Manuscripts are published online shortly after acceptance, before technical editing, formatting and proof reading. Using this free service, authors can make their results available to the community, in citable form, before we publish the edited article. We will replace this Accepted Manuscript with the edited and formatted Advance Article as soon as it is available.

You can find more information about Accepted Manuscripts in the author guidelines.

Please note that technical editing may introduce minor changes to the text and/or graphics, which may alter content. The journal's standard Terms & Conditions and the ethical guidelines, outlined in our author and reviewer resource centre, still apply. In no event shall the Royal Society of Chemistry be held responsible for any errors or omissions in this Accepted Manuscript or any consequences arising from the use of any information it contains.

Journal Name

View Article Online
DOI: 10.1039/C7QI00645D

ARTICLE

Review of computer simulations on anti-cancer drug delivery in MOFs

Received 00th January 20xx,
Accepted 00th January 20xx

DOI: 10.1039/x0xx00000x

www.rsc.org/

Marianna Kotzabasaki[a] and George E. Froudakis[a†]

Metal-Organic Frameworks (MOFs) have been recently used as potential nanocarrier platforms in biomedical applications such as drug storage and delivery, due to their low toxicity, biodegradability, high internal surface area, widely tunable composition, high payloads and controlled drug release. In this review, we summarize the computational techniques that have been performed to study anti-cancer drug delivery in MOFs. Computational simulations can offer a unique insight into the drug adsorption and diffusion mechanisms in porous nanocarriers at the atomic level, since a clear molecular-level understanding is important for the development of novel drug delivery systems with better control of drug administration. The calculated drug loading capacities of the reported MOFs are in good agreement with the experiments, making these materias promising for drug storage with exceptional payloads. The simulations also revealed a slow drug release rate for the stated MOFs, reducing the side effects of the traditional medication and thus improving the life expectancy of the patients affected by cancer. This review study will be useful to identify the most auspicious MOFs in cancer therapy prior to experimental studies and to effectively design smart nanocarriers able to deliver chemotherapeutics specifically to the damaged cells and to release them in a controlled way, offering a primary virtue over conventional therapy.

1. Introduction

Cancer comprises more than 100 different types of diseases in which body's cells begin to divide uncontrollably.[1] No one knows the exact cause of most cases of cancer, but research has shown that certain risk factors may increase patients' chances to develop cancer over the course of their lifetime. The most common risk factors of developing most types of cancer include aging, tobacco, sun exposure, radiation exposure, chemicals and other substances, some viruses and bacteria, certain hormones, family history of cancer, alcohol, poor diet, lack of physical activity, or obesity.[2]

Cancer is among the dominant causes of death on a global scale. About 1 in 2 men and 1 in 3 women in the United States (US) will develop the disease at some point in their lives. In 2012, there were stated 14 million new cancer cases and 8.2 million cancer deaths worldwide.[2] According to the National Center for Health Statistics, in 2017, 1.688.780 new cancer cases and 600.920 cancer deaths are expected to happen in the US.[3] On the top of the list appears the breast cancer, with more than 255,000 new cases projected to occur in the US in 2017. The next most common types of cancer are lung and prostate cancer.[2]

Cancer can begin in every part of the human body, consisting of more than 30 trillion cells. Cancer cells differ from normal cells in various ways. Unlike normal cells, cancer cells don't stop growing and dividing, but they keep proliferating to form a tumor which is constantly growing in size. Moreover, cancer cells ignore signals which normally lead cells to apoptosis. Another important difference is that cancer cells are less specialized than healthy cells. Whereas cells usually undergo cellular differentiation to carry out a specific function in the body, cancer cells do not. In addition, normal cells stick together in the right place in the body, whereas cancer cells do not. So, they are detached from their neighbours and can spread to other parts of the body, causing metastatic cancer. Cancer cells are also able to escape the immune system, even though it normally eliminates abnormal cells from the body. Looking under a microscope, cancer cells are of variable size and some of them are larger than normal cells while other are smaller. Cancer cells also have an abnormal shape, both of the cell, and of the nucleus which appears both darker and larger than in normal cells.[4]

Cancer can be treated by surgery, radiation therapy, chemotherapy, immunotherapy, targeted therapy, hormone therapy, photodynamic therapy, stem cell transplant and precision medicine. The patients often receive only one of these therapies, but when the cancer is metastatic, a combined treatment is applied, such as surgery with chemotherapy and/or radiation therapy.[2]

German biochemist Paul Ehrlich introduced the term ''chemotherapy'' in the early 1900s, defining it as the use of

[a] Department of Chemistry, University of Crete, Voutes, 71003, Heraklion, Greece
† Corresponding authors. E-mail addresses: frudakis@uoc.gr Tel: 302810545056; fax: +302810545001 (G. E. Froudakis)
Electronic Supplementary Information (ESI) available: [details of any supplementary information available should be included here]. See DOI: 10.1039/x0xx00000x

This journal is © The Royal Society of Chemistry 20xx

chemicals to treat disease. Chemotherapeutics can destroy cancer cells by inhibiting their growth and reproduction. A series of chemicals were also tested for their potential anti-cancer activity using animal models, as proposed by Ehrlich. He was also interested in the development of anti-cancer drugs, including aniline dyes and alkylating agents.[5] The lightning development of cancer chemotherapeutics began in the 1940s. The first drugs were based on the nitrogen mustards which are nonspecific DNA alkylating agents and cause the death of cancer cells. During the same period, a second category of anti-cancer drugs came to light, the well-known antimetabolites, which inhibit a normal metabolic process in the body. These agents get embedded into DNA or RNA to interfere with the process of division of cancer cells and hence stop tumors growth.[6] As the development of these primary drugs was successful, many additional categories of chemotherapeutics have been used so far. Such categories are nitrosoureas, antitumor antibiotics, plant alkaloids, topoisomerase and mitotic inhibitors and steroid hormones.[7]

All types of chemotherapeutics can cause side effects such as anemia, appetite loss, thrombocytopenia, constipation, delirium, diarrhea, edema, fatigue, hair loss, infection and neutropenia, lymphedema, memory or concentration problems, nausea and vomiting, nerve problems, pain, fertility problems, skin and nail changes, sleep problems and urinary system problems.[2]

The main role of chemotherapy is to prevent the proliferation of cells so it affects both cancerous and healthy tissues which share the same DNA and major metabolic pathways. Thus, conventional chemo drugs are generally toxic to normal cells and can cause numerous side effects. The newer chemotherapeutic agents are more specific for tumor cells, without any further normal tissue toxicity.[6]

Nanoparticles as drug delivery platforms enable unique approaches to treat cancer, increasing the specificity of anti-neoplastic agents towards tumor tissues.[8,9,10,11,12] Over the past two decades, a variety of nanoparticle delivery systems have been proposed for anti-cancer targeting and treatment, comprising organic and inorganic materials.[13,14,15,16] Fig. 1. depicts many nanoparticle therapeutics that have been used for chemotherapeutic agents' delivery including polymer–drug conjugates, lipid-based nanoparticles, polymeric nanoparticles, protein-based nanoparticles, biological nanoparticles, and hybrid nanoparticles.[17] Cancer therapies based on nanoparticles can eliminate the major drawbacks of conventional chemotherapy including poor targetability, burst effects due to high doses and poor pharmacokinetics. These nanoparticles should be non-toxic, stable *in vitro* and *in vivo*, biocompatible, biodegradable and have controllable drug distribution and release.[18]

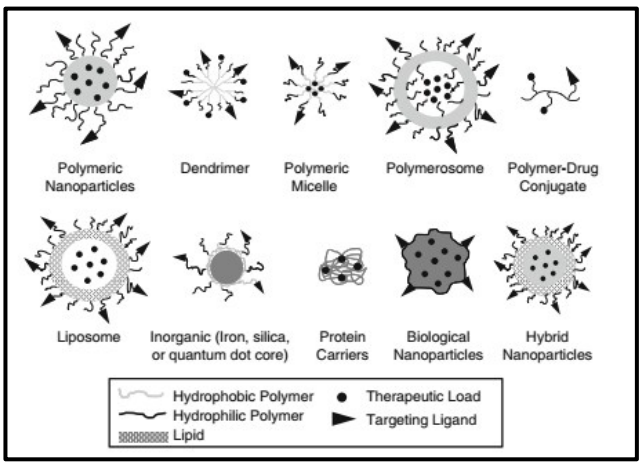

Fig.1 Nanoparticle platforms for drug delivery. Reprinted with permission of Springer from ref 17. Copyright Springer, Berlin, Heidelberg © 2010.

The drug targeting of these nanoparticles is a major challenge in cancer therapy. There are two major mechanisms to target anti-neoplastic agents using nanocarriers: Passive and active targeting. Unlike healthy tissues, tumors are featured by their leaky blood vessels and poor lymphatic drainage. Thus, nanoparticle therapeutics can efficiently penetrate tumor tissues. Passive targeting, therefore, is based on the accumulation of long-circulating nanocarriers in pathological sites with compromised vasculature via the enhanced permeability and retention (EPR) effect. In contrast, active targeting is based on specific interactions between the nanocarrier and receptors on the pathological cell, which may also promote incorporation of nanocarriers through receptor-mediated endocytosis.[19]

Surface modified (with ligands and other small or polymeric compounds) multifunctional nanoparticulate drug systems have been used for delivery of anti-cancer drugs to upgrade active and passive targeting, different release profiles as well as cell targeting and stimuli responsibility. These smart nanocarriers can transport the drug to the target tissue and once there, the presence of a certain stimulus, internal (pH, redox, enzymes, small molecules), or external (light, temperature and magnetic field), will trigger the release of the encapsulated drugs.[20] Siafaka *et* al. successfully synthesized a novel nanoparticle-based targeted drug delivery system comprising of folate-pegylated polyester nanoparticles entrapping the new anticancer drug ixabepilone for targeting folate receptor overexpressing breast cancer cells.[21] New thermosensitive nanoparticles have also been prepared by biocompatible pegylated aliphatic polyester block copolymers for local cancer treatment, enhancing drug delivery to the tumours following application of local hyperthermia (tumour heating at 42 °C).[22] The potential of poly(propylene succinate) copolymers with poly(ethyleneglycol) (PPSu-PEG) has also been investigated for the development of temperature-sensitive, targetable cisplatin nanocarriers.[23]

Nevertheless, most of the proposed nanoparticles investigated as drug carriers, suffer from important drawbacks such as low drug capacity and/or poor control of release kinetics. Recently, Metal-Organic Frameworks (MOFs) have been proposed as alternative nano-carrier platforms for drug delivery. MOFs are organic/inorganic hybrid materials composed of metal ions or clusters, interconnected through an organic linker.[24] These hybrid materials exhibit desirable characteristics as drug carriers, including low toxicity, good

This journal is © The Royal Society of Chemistry 20xx

biocompatibility and biodegradability, tunable host-guest interactions, exceptionally high internal surface areas and large pore sizes for drug encapsulation, stability in an aqueous environment and versatile functionality for post-synthetic grafting of drug molecules.[25,26,27,28,29]

Despite the progress in the synthesis and application of biocompatible MOFs for drug delivery, there is only a limited understanding of drug adsorption and release mechanism at the molecular level. Computational simulations can give a unique insight in the molecular behaviour of a drug molecule in porous materials that plays a key role in drug loading and release. The storage and release of drugs in porous nanovehicles is governed by a variety of factors including pore volume, surface functionalization, and interaction with the nanomaterial.[30,31] These physical properties can be reproduced and studied using computational techniques. Specifically, through density functional theory (DFT) calculations, it is possible to identify the most favorable conformations and adsorption sites.[28,32] Additionally, recent studies have proved the capability of Grand Canonical Monte Carlo (GCMC) simulations to predict the drug loading capacities of MOFs.[33] Lastly, Molecular Dynamics (MD) simulations have been carried out to study the diffusion of drugs within the pores, indicating that such simulations can be used for screening purposes prior to experimental investigation.[34]

Below, we review the molecular simulations used in the literature to investigate drug adsorption and diffusion in MOFs, emphasizing in anti-cancer drug delivery.

2. Simulation Methodology

Molecular simulations can complement experimental studies of drug adsorption and diffusion in porous systems. The term "molecular simulations" refers to computational methods in which the molecular properties of a system are explicitly taken into account. These methods play an important role in the study of the behavior of microscopic and macroscopic processes such as adsorption, since they use statistical mechanics to model the thermodynamic properties of the system under study.

There are different types of computational methods using quantum mechanics or classical mechanics as their approach. Quantum mechanics (QM) itself can be divided to *ab initio* and semi-empirical methods. In the *ab initio* calculations, an electronic wavefunction model is chosen to solve the Schrödinger equation. Fundamental constants and atomic numbers of the nuclei are used as the only input values. On the other hand, semi-empirical methods use a simplified form of the Hamiltonian operator with some parameters taken from experiments. While the former is computationally very expensive and time consuming for the large systems of particles and its accuracy merely depends on the employed model for the wavefunction, the latter approach is less accurate but more reasonable to be used for large systems.[35]

Classical approaches comprising different types of calculations such as Monte Carlo (MC), Molecular Dynamics (MD) and Molecular Mechanics (MM) which are based on empirical models to describe the interactions between atoms or molecules. These methods are

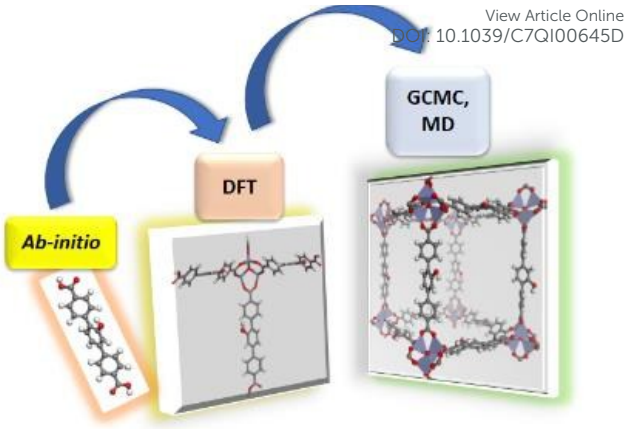

Fig. 2 Multi-scale methodology scheme, showing the different levels of theory and the corresponding size of systems under study.

taking the advantage of treating large molecular systems with thousands of atoms since they are computationally inexpensive compared to *ab initio* methods. The major drawback of these methods is the dependence of their accuracy and results on the parameters that are used to describe the interatomic potential between atoms and molecules. Moreover, some of classical methods are taking into account only the pressure and temperature dependence of the simulations, while others can calculate the time dependant thermodynamic properties of the system as well as the configuration of the particles at any time.[36]

Over the last years, multiscale modeling of various physical and chemical phenomena like adsorption, chemical reactions and diffusion has been developed. Multiscale modeling consists of different levels of theory depending on the length of the system under study and the time evolving a physical phenomenon. The different levels are usually distinguished as described in Fig. 2: The 1st level of QM models consists of the smaller molecular fragments of the periodic MOF structure and is used for calculating the interaction between host MOF and drug molecules. The 2nd level of classical models consists of the entire MOF periodic structure with thousands of atoms and is used for studying the adsorption and diffusion of drug molecules within MOF structures.[37]

In what follows we give an introductory review of the theoretical techniques that are in our view most relevant to the treatment of drug adsorption and diffusion in MOFs.

2.1 Quantum Chemical Methods

Electronic structure calculations on MOFs are generally aimed at making first principles predictions of a wide range of physical and chemical properties while are limited by the available computational power. To overcome this problem, density-functional theory (DFT) methods have been developed. These calculations use approximations to make the calculations feasible but without the need of *a priori* assumptions which would compromise the first-principles approach. Some recent reviews on the Quantum Chemical characterization of the properties of MOFs are those of Odoh *et* al.,[38]Jiang,[39] Coudert *et* al.[40] and many others.

DOI: 10.1039/C7QI00645D

2.1.1 Density Functional Theory (DFT)

There are various numerical methods to determine the electronic structure of the molecules, such as Hartree-Fock (HF) method. However, this method does not take into account the effect of electron correlation. It means that the instantaneous coulombic interactions as well as the quantum mechanical effects on the electron distributions are neglected.[31] Consequently, in molecules with many electron atoms, HF methods does have accuracy limitations.

In this regard, a method which is widely being used, is DFT, in which the total energy is expressed in terms of the total electron density, rather than the wavefunction. This method does consider the important effect of electron correlation and simultaneously is applicable to big molecules while it has smaller computational demands. However, DFT has deficiency in describing then non-local dispersion forces induced by electron correlations. The most widely used GGAs – the so-called Perdew-Burke-Ernzerhof (PBE)[41] functional claims to treat the long-range interactions fairly. A general empirical dispersion correction has been proposed by Stefan Grimme[42] for DFT calculations, predicting more accurately the energetics in systems where dispersion is important.

Applying DFT calculations to study anti-cancer drug delivery in MOFs, it is possible to describe precisely specific host–guest interactions and identify the most favorable conformations and adsorption sites between host MOFs and guest drug molecules.[28,32]

2.1.2 Semi-empirical Methods

Semi-empirical methods are based on HF method, but make many approximations and adopt some parameters from empirical data. These calculations can be used to treat large molecular systems, as the two-electron integrals of the Hamiltonian are not explicitly considered, reducing the computational cost without a major impact on the accuracy. Only the valence electrons of the system are explicitly included, whereas the core electrons are subsumed into the nuclear core which is replaced by a parameterized function. By considering all valence electrons these methods differ from those theories (e.g. Hückel theory) that explicitly consider only the π-electrons of a conjugated system and which are therefore limited to specific classes of molecules.[43]

The virtue of semi-empirical calculations is that they are much faster than the *ab initio* calculations. The challenge of semi-empirical calculations is that the results can be slightly defective. If the molecule being computed is similar to molecules in the database used to parameterize the method, then the outcomes may be very good. If the molecule being computed is significantly different from anything in the parameterization set, the results may be very poor.

Performing semi-empirical methods to study anti-cancer drug delivery in MOFs, it is possible to identify the most favourable conformations of larger molecular fragments of host MOFs with respect to large drug molecules but without the same accuracy as performing DFT calculations on smaller molecular fragments of the structure.

2.2 Classical Methods

Many of problems that we want to unravel in molecular modelling are unfortunately too large to be considered by QM methods. Force Field methods (also known as molecular mechanics, MM) ignore the electronic motions and compute the structure and energy of molecules based on nuclear motions only. MM is mainly used to perform calculations on systems containing a large number of atoms.

2.2.1 Molecular Mechanics (MM)

The molecular mechanics (MM) energy expression consists of a simple algebraic equation for the energy of a compound. The constants in this equation are obtained either from experimental data or *ab initio* calculations. Crucial for the success of an MM method is the database of compounds used to parameterize the method (a set of parameters and potential functions is called a Force Field, FF). MM is computationally less demanding than the QM, so in many cases large molecular systems can be modelled successfully, but on the other hand, it fails in description of the electronic structure of the molecule.[43]

One important application of MM techniques in structural biology is the simulation of the docking of a ligand molecule onto a receptor.[44] The molecular docking approach is distinguished in two main parts: A search algorithm to determine all possible optimal conformations for a given complex (protein-protein, protein-ligand) in an environment and a scoring function to evaluate the binding energies between the parts of the complex. It's a powerful technique for structure-based drug discovery. Recent molecular docking studies were carried out to estimate the binding conformation and binding affinity of guest drug molecules to host MOFs.[45]

2.2.2 A simple Molecular Mechanics Force Field (FF)

In principle, a set of specific equations for calculating the potential energy between interacting atoms combined with the related parameters and partial atomic charges are called force field (FF). In MM methods, classical definitions of potential energy are used. In this regard, two main types of molecular interactions are distinguished: Intermolecular interactions which occur among the individual molecules and intra-molecular interactions that are contributions of atoms into the potential energy within each molecule.

Intermolecular potential interactions relate to the non-bonded interactions among various atoms from different molecules. This class of interactions can be categorized as long-range and short-range interactions which means how fast they fall off with respect to distance. Electrostatic interactions and Van der Waals (vdW) interactions are two contributors in this part. For the electrostatic interactions, atomic charges in MOFs need to be calculated by QM methods. VdW potential parameters can be determined from experimental or QM data. In the last case, the binding energies between drug molecules and host MOFs are evaluated by QM methods and then an analytic potential function is adopted to fit the binding energies.

Intra-molecular interactions concern the potential interactions among the atomic components of every molecule. This includes the bond stretching, angle bending, dihedral motions (torsional rotation)

This journal is © The Royal Society of Chemistry 20xx

and out of plane bending (inversion) potentials. Moreover, vdW interactions between all the atoms which are not separated by three or more covalent bonds should be also taken into account.

Standard modern FFs choose similar definitions with slight variations to define total potential energy as the following equation:[46]

$$U = \sum_{Stretch} U_{ij} + \sum_{Bent} U_{ijk} + \sum_{dihedral} U_{ijkl} + \sum_{out\ of\ plane} U_{ijkl} + \sum_{L-J} U_{ij} + \sum_{Electrostatic} U_{ij}$$

There are numerous FFs developed for different desires. Among those are MM2, MM3, MM4, CHARMM, OPLS, GROMOS, CVFF, TraPPE and many others. Universal Force Field (UFF)[47] and DREIDING[48] have been widely used for MOFs, while Assisted Model Building and Energy Refinement (AMBER)[49] is widely used for proteins, DNA and drug molecules.

2.2.3 Grand Canonical Monte Carlo (GCMC)

Monte Carlo (MC) simulations are well suited to study the thermodynamics of adsorption in nanoporous materials. In particular, recent studies have proved the capability of Grand Canonical Monte Carlo (GCMC) simulations to predict the drug loading capacity of MOF structures.[31,33] In GCMC ensemble (μ, V, T) the chemical potential, μ, the volume, V, and the temperature, T, are kept constant, while the number of molecules, N, is allowed to vary. The chemical potential can be calculated by an appropriate equation of state[50] or from the Widom[51] method.

During these simulations, the following trial moves are tried: particle creation, particle deletion and particle rotation and/or displacement. Due to particle creation and deletion, the number of molecules, N, within the pore varies, whereas these moves must be tried with the same frequency. For each trial, if the final configuration of the system is lower in energy than its predecessor, the move is accepted. If the new configuration is higher in energy than the previous, the energy difference of the configurations before and after the trial move is used for the calculation of the possibility of accepting the trial move.[52]

There are many interatomic potentials to describe the vdW interactions. The most common form to express the vdW forces is by using the Lennard-Jones (L-J) model[53] as follows:

$$U_{LJ}(r_{ij}) = 4\varepsilon_{ij}\left[\left(\frac{\sigma_{ij}}{r_{ij}}\right)^{12} - \left(\frac{\sigma_{ij}}{r_{ij}}\right)^{6}\right]$$

, where σ is the L-J size parameter, and ε is the potential well depth at a separation distance of $r_{min}=2^{1/6}\sigma$, so $U(r_{min})=-\varepsilon$. The parameters ε and σ are specific for every kind of atom and can be either taken from the literature or calculated from *ab initio* methods. Once the potential parameters, ε and σ, for a given atom type have been evaluated, the Lorentz-Berthelot mixing rules are usually computed for the calculations of these parameters for a pair of different atoms:

$$\varepsilon_{ij} = \sqrt{\varepsilon_{ii}\varepsilon_{jj}}, \quad \sigma_{ij} = \frac{\sigma_{ii}+\sigma_{jj}}{2}$$

View Article Online
DOI: 10.1039/C7QI00645D

The L-J potential was improved by the Buckingham potential later proposed by R. A. Buckingham[54], in which the repulsive part is an exponential function:

$$V_B = \gamma\left[e^{-r/r_0} - \left(\frac{r_0}{r}\right)^6\right]$$

, where γ is a suitable constant.

The electrostatic interactions are usually described by the common Coulomb potential:

$$U_{elec}(r_{ij}) = \frac{1}{4\pi\varepsilon_r\varepsilon_0}\frac{q_i q_j}{r_{ij}}$$

, where ε is the electric constant of the medium where the charges are placed, ε_0 is the permittivity in the vacuum (8.85×10^{-12} C^2 s^2 kg^{-1} m^{-3}), q_i and q_j are the charges of the interacting atoms and r_{ij} the distance with the atoms i and j.

The major outputs of a GCMC simulation are the configurations of the system in given conditions, the absolute adsorption uptake (N_{ads}) and the isosteric heat of adsorption (Q_{st}) as follows:

$$Q_{st} = RT - \frac{\langle UN\rangle - \langle U\rangle\langle N\rangle}{\langle N^2\rangle - \langle N\rangle^2}$$

, where the brackets denote the average over the configurations, N is the number of adsorbed drug molecules in host MOFs and U is the total energy.

2.2.4 Molecular Dynamics (MD)

Molecular dynamics (MD) use Newton's laws of motion to examine the time-dependent behavior of molecular systems. Since these calculations are interested in the time evolution of the particle, the equation can be expressed in terms of displacement r with respect to time t:

$$\frac{F_i}{m_i} = \frac{d^2 r_i}{dt^2}$$

MD employs an initial configuration of the molecules as input, and then computes the molecular forces based on interaction parameters of a given FF. Subsequently, it determines velocities and positions of the molecules by integrating the Newton's law of motion. Data collected from any preceding step is used to calculate the new forces, velocities and positions for the ensuing configuration after a very small-time interval. This procedure is followed by the same cycle to predict the configuration of the system at any time in the future. This means that MD generates a trajectory of the system with respect to time. This trajectory can be obtained by integrating over several finite difference schemes. In particular, the Verlet algorithm is probably most widely used. Using a Taylor expansion, the velocity Verlet algorithm can be easily derived:

$$r(t+\Delta t) = r(t) + V(t)\Delta t + a(t)\Delta^2 t$$

The time step Δt is chosen such a way that the integration is accurate enough and the total energy of the system is conserved. The thermodynamic averages of the system can be calculated from the trajectory obtained over a sufficient period of time, by applying statistical mechanics approach to resemble the thermodynamic properties of the macroscopic system of interest.[55]

MD can be used to study the diffusion of guest molecules inside adsorbent materials. In particular, MD simulations have been employed to study the diffusion of drugs within MOF pores, indicating that such simulations can be used for screening purposes prior to experimental investigation.[56]

3. MOFs as anti-cancer drug delivery systems

3.1 Metal-Organic Frameworks (MOFs)

Batten and co-workers[57] recommended a hierarchical terminology where the most general term is coordination polymer (CP). CPs are inorganic-organic hybrid materials composed of metal ions linked by organic ligands that form an extended structure. Coordination networks (CN) are a subset of CP and metal-organic frameworks (MOFs) are a further subclass of CN (Fig. 3). According to the International Union of Pure and Applied Chemistry (IUPAC), "a Metal-Organic Framework, abbreviated to MOF, is a Coordination Polymer (or alternatively Coordination Network) with an open framework containing potential voids".[57]

The first MOF which showed permanent porosity and didn't collapse upon removal of the guest molecules from the pores, was reported by S. Kitagawa *et* al.[58] in 1997. They examined the reversible adsorption of small molecules (N_2, O_2, CH_4) in the microporous cobalt-bipyridyl complex $[Co_2(bipy)_3(NO_3)_4]_n$.

In 1998, S. Kitagawa[59] suggested a classification of porous coordination polymers into three categories — first, second and third

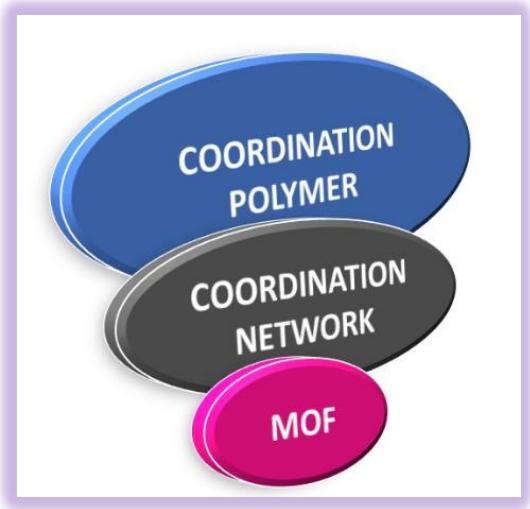

Fig. 3 Hierarchical terminology of coordination polymer, coordination network and metal-organic framework by IUPAC.

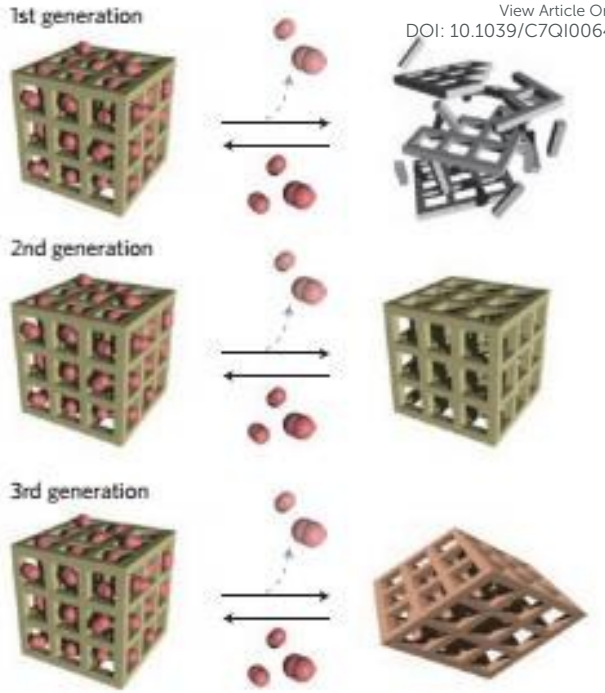

Fig. 4 Classification of coordination polymers in three generations according to S. Kitagawa. Reprinted by permission from Macmillan Publishers Ltd: [Nature Chemistry] (ref59), Copyright (2009)

generations, due to their structural properties (Fig. 4). The 1st generation represents materials whose frameworks irreversibly collapse upon removal of guest molecules. The 2nd generation represents materials whose frameworks are robust and keep their porous structures even after guest removal. The 3rd generation materials have flexible, dynamic frameworks, which are subjected to structural transformation as response to external stimuli (e.g., temperature, electric field or guest molecules' adsorption) and exhibit high potential for different applications.

In 1999, O. M. Yaghi and co-workers[60] synthesized a prototypic framework, the so-called MOF-5 ($[Zn_4O(bdc)_3]_n$) which became a nuclear for the expeditious development of robust and highly porous MOFs. To date, more than 15259 documents about MOF research have been published according to Scopus database (Fig. 5). Despite

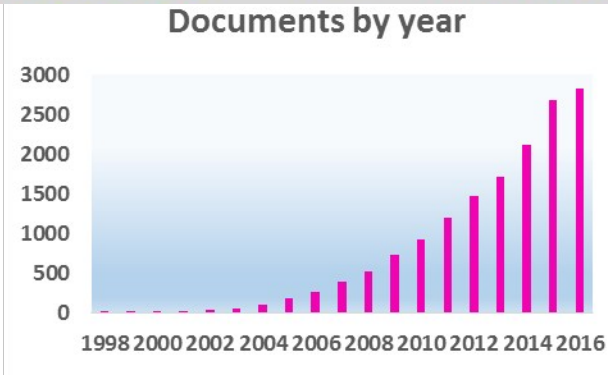

Fig. 5 Number of publications featuring the term "metal-organic frameworks" in their topics (Source: https://www.scopus.com).

This journal is © The Royal Society of Chemistry 20xx

View Article Online
DOI: 10.1039/C7QI00645D

ARTICLE

MOF trade name (structure)	Ligand	Formula	S_{BET}[a]/m^2 g^{-1}	Pore dimensions[a]/Å
Basolite F 300	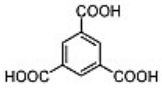	Fe(BTC)	840	21
Basolite C 300 (HKUST-1)	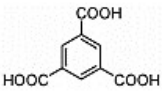	$Cu_3(BTC)_2$	1019	11, 16 and 6
Basolite A 100 (MIL-53(Al))	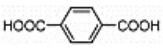	Al(OH)(BDC)	950	8.5
Basolite Z 1200 (ZIF-8)		$Zn(MeIm)_2$	1947	11.6

[a] Nitrogen adsorption isotherms were measured by us at 77 K on a Micromeritics ASAP 2000 volumetric adsorption analyser. Before the measurements, the samples were degassed for 4 h at 473 K. The specific surface area was calculated by applying the BET model to the nitrogen adsorption data.

Table 1 Structural composition, textural and physical properties of MOFs commercialized by BASF. Reproduced ("Adapted") from (Ref 61) with permission of The Royal Society of Chemistry.

the vast number of MOF structures, the commercially available MOFs are limited. A few examples of MOFs commercialized by BASF are presented in Table 1, while the surface area and pore dimensions of these materials are also given.[61]

MOFs offer significant potential for a range of applications and during the last decades, their potential applications were in focus of investigations in the fields of gas storage/separation, catalysis, sensing, drug delivery, etc. One of the most promising application that we will focus on this review is the utilization of MOFs in anti-cancer drug delivery.

3.2 The first experimental studies of MOFs as potential drug carriers

In 2006, Horcajada *et* al.[26] investigated the first MOFs' family (Table 2)[62] that can be used as potential drug carriers. The two MOFs studied, MIL-100 and MIL-101 (MIL is abbreviation of Materials of Institute Lavoisier) are composed of trivalent metal centers with carboxylic bridging ligands and possess large pores with large surface areas. These structural characteristics promote MILs' use as efficient drug carriers. They carried out experiments to study the loading and release kinetics of the analgesic drug, Ibuprofen (IBU), in both MILs' structures. The loading capacity of IBU in MIL-100 reached 0.347 g IBU/g MOF and in MIL-101 1.376 g IBU/g MOF. The difference may be attributed to the volume of each cage for MIL-101 (12700 Å^3 and 20600 Å^3) and for MIL-100 (8200 Å^3 and 12700 Å^3). The release behavior of IBU in two MOFs was also investigated and was slow enough to reduce the side effects of the conventional medication.

MOF	Drug	Loading (%)	Application
MIL-100(Cr)	Ibu	35	Anti-inflammatory/ analgesic
HKUST-1(Cu)	Nimesulide	20	
MIL-101(Cr)	Ibu	1.38[a)]	Anti-inflammatory
MIL-53(Cr)		22	
MIL-53(Fe)		21	
UiO-66(Zr)		35	
$Zn(BDC)(H_2O)_2$		45	
MIL-101(Fe)	ESCP	13	Antitumoral
MIL-100(Fe)	Doxo	9	
Zn(bix)		21	
MIL-100(Fe)	Bu	25	
Zn(bix)	Camptothecin	21	
Zn(bix)	Daunomycin	21	
ZIF-8(Zn)	5-FU	45	
Zn-based MOF (TATAT chiral linker)		50	
MOF-1(Zn)		37	
MOP-15(Cu)		24	
Cu-BTC(Cu)		82	
MIL-100(Fe)	CDV	16	Antiviral
MIL-101_NH_2(Fe)		42	
MIL-100(Fe)	AZT-Tp	24	Antiretroviral
MIL-101_NH_2(Fe)		42	

Table 2 Drugs encapsulated in different MOFs. Reprinted with permissic from ref 62. Copyright Wiley-VCH Verlag GmbH & Co. KGaA © 2015

View Article Online
DOI: 10.1039/C7CC00645D

MIL-100 showed initial release within two hours with full release after three days, while MIL-101 showed steady release for eight hours with full release after six days.

MIL-53 is another MOF in the MIL family that adsorbs around 20 wt% of IBU and has properties that make it desirable for long release (3 weeks) medications.[32]

MILs family have hydrophobic pores, but what about MOFs that use hydrophilic pores? The hydrophilic pores will hold a positive or negative charge, and the drug used will contain opposite charges to the host MOFs. The Rosi[63] group created a MOF consisting of zinc(II) ions, adenine, and para-biphenyl-dicarboxylic acid. This MOF can be cationically triggered to release the drug contained inside. It was loaded with a hydrochloride salt of the antiarrhythmic procainamide (PROC). The complete loading (0.22 g PROC/g MOF) was achieved after 15 days, and a steady cation-triggered PROC release was observed within 20 h, while a complete release was observed after 72 h.

Furthermore, other biocompatible MOFs have also been studied as promising materials for drug storage and controlled drug release. A few examples of such applications and the drug loading capacity of the mentioned MOFs are presented above in Table 2. Sun *et* al. achieved the highest loading of 50 wt% of the antitumor agent 5-FU using a Zn-MOF containing an achiral ligand.[64]

In the following section, we will review the applications of MOFs in cancer therapy and drug delivery.

3.3 MOFs as anti-cancer drug carriers

Emphasising the tremendous research interest in the field of cancer therapy, most of the reported studies dealing with the encapsulation and release of drugs using MOFs, concern antitumor agents.

The first examples of nanoMOFs (nMOFs) platforms to deliver platinum chemotherapeutics have been reported by Lin group (Table 3).[65] In 2008 Rieter *et* al.[66] synthesized a nMOF designated as NCP-1, constructed from Tb^{3+} ions and disuccinatocisplatin (DSCP). NCP-1 was further encapsulated in shells of amorphous silica to enhance stability and was functionalized with c(RGDfk) to target an integrin over expressed in many cancers. In physiological media, the framework was decomposed and the cisplatin prodrug was released slowly by diffusing out of the silica shell in a more toxic form to kill cancer cells. In 2009, Taylor-Pashow *et* al.[67] loaded an iron aminoterephthalate nMOF (SiO_2-MIL-101_NH_2) with 13 wt% of ethoxysuccinato-cisplatin (hydrophobic prodrug of cisplatin) and an image agent (a BODIPY dye). These cargoes were released upon the degradation of the nMOF framework, and the release rate of the cargo was controlled by coating the nMOF particles with a silica shell.

Horcajada *et* al.[68] loaded other chemotherapeutic drugs, busulfan (Bu) and doxorubicin (DOX), in a series of different non-toxic porous iron carboxylate nMOFs. In the case of Bu, MIL-89, MIL-88A, MIL-53 and MIL-100 showed high drug loading capacity, reaching up to 25 wt% loading in the case of MIL-100, outperforming other conventional lipid and polymeric drug carriers. Bu was however rapidly released from MIL-100(Fe) with a burst effect of 60% in the first 30 minutes, which can be attributed to the fast drug diffusion through the 3D mesopores of the structure. Later, Chalati *et* al.[69] encapsulated Bu in the flexible MIL-53, slowing down the drug release rate from its hydrophobic 1D-porous system.

chemotherapeutic agents	
NMOFs	
Fe-BDC (MIL-101)	cisplatin
ZIF-8	cisplatin, DOX, 5-Fu', CPT, Topotecan
Zr-UiO-68	cisplatin
Gd-BDC	MTX
Zn-bix	DOX
Fe-imidazole	DOX
Gd-BDC	DOX
MIL-100(Fe)	DOX
Zn-hexadentate	5-Fu'
Cu-BDC	5-Fu'
Zn-1,2,3,4,5,6-hexakis(3carboxyphenyloxymethylene)benzene	5-Fu'
Cu-bipy	5-Fu'
POM©ZIF-8	5-Fu'
Cu-BTC	5-Fu'
Zr-UiO-66	alendronate
Cu-BTC	COX-2
Zn/Cu-3,5-bis(pyridine-3ylmethylamino)benzoic acid	cytotoxic 3,5bis(pyridine-3ylmethylamino) benzoic acid
NCPs	
Tb-DSCP	cisplatin
Zr-DSCP/La-DSCP	cisplatin
Zn-cis/Zn-oxali	cisplatin/oxaliplatin
Zn-oxali and GMP	oxaliplatin and gemcitabine
Prussian Blue	cisplatin
Zn-MTX/Zr-MTX/Gd-MTX	MTX
Ca-pamidronate/zoledronate	pamidronate, zoledronate

Table 3 Examples of NMOFs and NCPs for Cancer Therapy. Reprinted with permission from {C. He, D. Liu and W. Lin, *Chem. Rev.*, 2015, **115**(19), 11079–11108}. Copyright {2015} American Chemical Society.

Regarding DOX, MIL-100(Fe) showed a drug loading capacity of 9 wt% with a sustained release profile over 14 days.[68] Recently, Anand and co-workers[70] revealed the formation of host-guest interactions between DOX and the iron metal sites of MIL-100 nanoparticles (NPs), proofing the abovementioned slow release rate. Vasconcelos *et* al.[71] encapsulated DOX into the zeolitic imidazolate framework (ZIF-8) with high-load (49 wt%) and progressive release (66% of the drug released after 30 days). DOX was also successfully incorporated into the ZIF-8 NPs in high payloads (52 wt%) and released in a controlled manner under internal pH stimuli, revealing a smart drug delivery system.[72]

This journal is © The Royal Society of Chemistry 20xx

NMOF	Drug	Loading percentage [wt]	Release time
MIL-100 (Fe)	DOX	9	14 days (PBS)
	Bu	25	—
$NaYF_4$:Yb/Er@MIL-100(Fe)	DOX	17.2	35 days (PBS)
MIL-101 (Fe)	Cisplatin prodrug	12.8	3 days (PBS)
ZIF-8	5-Fu	39.8	7 days (PBS)
	DOX	4.67	30 days (66%, DI water)
	CPT	2	—
PAA@ZIF-8	DOX	65.5	60 h (35.6%, PBS)
C@ZIF-8	5-Fu	23.1	50 h (PBS)
Zn-TATAT	5-Fu	33.3	7 days (PBS)
UiO (Zr)	Cisplatin prodrug	12.3	24 h (34%, PBS)

Table 4 NMOF-based drug delivery systems. Reprinted with permission from ref 74. Copyright Wiley-VCH Verlag GmbH & Co. KGaA © 2015.

Recently, Qian *et* al. synthesized two zinc-based MOFs, named as ZJU64 and ZJU-64-CH3.[73] Anticancer drug methotrexate (MTX) was encapsulated into the two MOFs, with a loading capacity of 13.45 and 10.63 wt% for ZJU-64 and ZJU-64-CH3, respectively. The same amount of MTX was released from MTX-loaded ZJU-64 and ZJU-64-CH3 at 37 °C for 72 h, but only took approximately 1.5 and 6 h at 60 °C, suggesting ZJU-64 and ZJU-64-CH3 as potential temperature-responsive drug carriers.

Despite the several experimental attempts to incorporate chemotherapy drugs into nanoscale MOFs and CPs and estimate the drug loading and release kinetics (Table 4),[74] there is only a limited understanding of anti-cancer drug adsorption and release mechanisms at the molecular level. In the following section, we will summarize the few studies used computational methods to study drug−MOF energetics and dynamics, giving a further insight in the molecular behavior of a drug molecule in porous materials that plays a key role in anti-cancer drug delivery.

3.4 Screening MOFs using molecular simulations

Molecular simulations are a useful tool to seek for an optimal MOF structure with high performance in drug delivery. In particular, with DFT calculations it is possible to identify the host-guest interactions between host MOFs and the adsorbed drug molecules and to calculate the binding energy of the MOF-drug complex. In addition, the GCMC simulation is the preferred method for simulating drug adsorption in MOFs' pores, while MD simulation is the ideal method to study drug diffusion from MOFs' pores under different thermodynamic conditions. However, the simulation concerning large drug molecules is challenging and that justifies the few computational studies on anti-cancer drug delivery in porous MOFs that we will summarize in the next section.

Moreover, this review suggests new computational tools that allow the study of new porous solids as potential drug delivery vehicles prior to experimental studies.

3.4.1 Simulations on anti-cancer drug delivery

3.4.1.1 5-FU

Liu et al.,[75] recently presented a combined experimental and computational study of three novel MOFs for the drug delivery of 5-FU. They applied GCMC simulations at 300 K to explore the host-guest interactions and to explain the loading capacity & controlled release characteristics of host materials. In particular, they synthesized three large nanocage-based porous MOFs with chemical formulae $[(Sm_3(L1)_2(HCOO)_2(DMF)_2(H_2O)]\cdot 2DMF\cdot 18H_2O$ (1), $[(Cu_2(L2)(H_2O)_2]\cdot 2.22DMA$ (2) and $[(Zn_2(L1)(DMA)]\cdot 1.75DMA$ (3) and subsequently they investigated their 5-FU adsorption capacity and release kinetics, comparing the experimental with the theoretical results. These MOFs have large adsorption capacity of 5-FU & release it in a controlled manner. The experimental studies showed that 5-FU was encapsulated in 1, 2 and 3 materials with high loadings of 40, 42, 45 wt%, respectively and the release rates were 72%, 96% and 79% of the drug after 96h in 1, 120h in 2 and 96h in 3, respectively. The theoretical results reproduced the experimental loading capacity of each MOF, revealing for the three structurally different frameworks nearly the same 5-FU adsorption amounts. They explained it by showing that the calculated 5-FU loading is related to the free volume of the structures. Combining experimental with computational approach is a promising technique for deeply understanding the molecular behavior of anti-cancer agents in porous materials.

J. Wang *et* al.[76] also reported a combined experimental-theoretical insight in the 5-FU delivery of two novel MOFs. The carried out GCMC simulations at 298 K to investigate the drug loading capacity of each material and the MOF-drugs interactions. Specifically, two isostructural nMOFs with chemical formulae $[Zn_3(\mu_3\text{-}O)(BTC)_2(H_3O)]_n$ (NTU-Z11) and $\{[Zn_3(\mu_3\text{-}O)(BTC)_2(DMF)]\cdot 2NH_2(CH_3)_2\cdot 4H2O\}_n$ (GDMU) (BTC =1,3,5-benzenetricarboxylate) were synthesized and the experimental loading of the 5-FU in the materials was around 38 wt% for NTU-Z11 and 22 wt% for GDMU. The high loading capacity of these MOFs was reproduced well by molecular simulations and the calculated loading was 40 wt% for NTU-Z11 and 20 wt% for GDMU. These results evinced a notable different loading capacity for NTU-Z11 and GDMU due to their different pore spaces. Comparison between calculated drug loading values and some structural properties of the frameworks confirmed that drug adsorption capacity is highly related to the void space of materials. Moreover, NTU-Z11 showed a pH-triggered controlled drug release profile that may be a useful characteristic of a smart drug delivery system for solid tumor targeting. The sustained release of 5-FU from both structures was confirmed by GCMC simulations that showed high Q_{st} values at about 28-35 kcal/mol for NTU-Z11 and at 38-54 kcal/mol for GDMU. The

later, showed higher Q_{st} values at high loadings due to the presence of solvent molecules in the structure. This combined experimental-computational study is a useful approach for recognizing promising structures that can act as carriers with high performance in drug delivery.

Li *et* al.,[77] proposed an interesting experimental and theoretical study of 5-FU delivery in a biocompatible MOF carrier containing a pharmaceutical ingredient linker, named as $\{[Zn_2(fer)_2]\}_n$ (H_2fer=ferulic acid) (1). Drug adsorption experiments revealed high amount of 5-FU (39 wt%) adsorbed in 1, which is in agreement with the GCMC adsorption isotherms at 298 K that exhibited remarkable drug loading capacity of about 50 wt% for 1. The simulations investigated the key drug-MOF interactions and the distribution of 5-FU within the MOF's pore, explaining the loading capacity & controlled release characteristics of 1. According to Radial distribution function (RDF) graphs, it is clear that the hydrogen bonding interactions between 5-FU and 1 control the loading of the drug, prolongating its drug release process. The calculated Q_{st} value of around 19-23 kcal/mol is suitable for drug adsorption and delivery with a slow release. The simulations also indicated that the adsorption energies are constant when drug loading changes, leading to a long-term release stability of the drug. Experimental studies also confirmed a slow release and controlled delivery of 5-FU which occurred within 100 hours in Phosphate-buffered saline (PBS, pH=7.4). Comparing the drug release profiles in acidic conditions, the results implied that the release of 5-FU can be decreased during blood circulation and its release rate gets increased into tumors. This combined experimental-computational study is a powerful technique to describe drug adsorption in porous materials, explaining and predicting the experimental trend.

Liu *et* al.,[78] suggested two isoreticular MOF structures with chemical formulae $Cu(L)(4,4'\text{-bipy})(H_2O)]_n{\cdot}1.5_nCH_3CN$ (1) and $[Cu(L)(4,4'\text{-bipy})(H_2O)]_n{\cdot}4nH_2O$ (2), H_2L = diphenylmethane-4,4'-dicarboxylic acid) as potential drug carriers for 5-FU delivery. The experimental loading of the drug into the framework 1 was around 27.5 wt%. 5-FU was released in a slow and controlled manner with 61 % of the drug released after 95 hours. The release kinetics of 5-FU consists of three stages: Initially, 21% of the loaded drug is released in the first 11 h, and then 51% is released in two slower stages. Furthermore, molecular docking calculations were performed to reveal the favorable arrangement of 5-FU molecules within the MOFs' pores (Fig. 6). These calculations provided a structural insight into the 5-FU sustained release from framework 1. Fig. 6 derived from docking approach, depicts a tight fitting of 5-FU into the pores of 1, suggesting that interactions between Lewis acid sites in 1 & base sites in 5-FU are the driving force for prolonged release of 5-FU.

F. M. Wang *et* al.[79] reported a combination of experimental and molecular simulations studies on a new MOF, named $\{[Co_2(L)(4,4'\text{-Bipy})_2]\cdot CH3CN\}_n$ (1) (H_4L = 5,5'-(biphenyl-4,4'-diyl bis(methylene))bis(oxy)diisophthalic acid, 4,4'-Bipy = 4,4'-bipyridine), as an auspicious carrier for 5-FU delivery. The experimental loading of the drug into 1 was around 15.0 wt%. In addition, they performed semiempirical AM1 calculations to investigate the adsorption mechanism of 5-FU to 1 at the molecular level and the calculated loading was about 12.7 wt%, which is little lower value than the experimentally measured one. They also presented a pH-triggered controlled drug release from 1.

Article Online
DOI: 10.1039/C7QI00645D

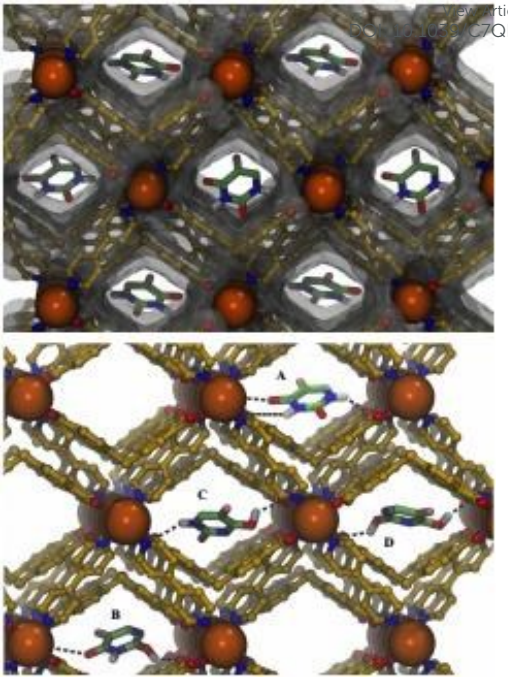

Fig. 6 Predicted conformation of 5-FU upon binding to framework 1. Top: Representation of the main diketo tautomer bound to the inner space of the pore defined by molecular (van der Waals) surface of the framework. Bottom: Predicted conformations of 5-FU tautomers upon binding to framework 2. Tautomeric forms are A) diketo, (B-C) keto–enol, and D) dienol. Reproduced ("Adapted") from (Ref 78) with permission of The Royal Society of Chemistry.

The results obtained from these theoretical investigations revealed that MOFs' structures can load high amounts of drugs and release them in a progressive way, acting as auspicious nano-encapsulators. In this regard, Q_{st} values of about 20-50 kcal/mol are suitable for drug adsorption and delivery with a slow release ("binding without overbinding"). Moreover, molecular simulations provided a further motivation for designing other similarly structured biocompatible, non-toxic MOFs which can offer equally superior drug loading and drug release properties.

3.4.1.2 Paclitaxel (Taxol)

Filippousi *et* al.,[80] studied the potential use of two biocompatible and biodegradable nMOFs, UiO-66 and UiO-67, as promising anti-cancer platforms for the taxol delivery. Hydrophobic taxol was adsorbed in both MOF structures and the experimental loading was around 140 mg/g in UiO-66 and 100 mg/g in UiO-67. In addition, the *in vitro* drug release studies revealed that the drug release depends on the drug-MOF interactions, while the prolonged release can be attributed to the further encapsulation of nMOFs in non-toxic polymeric microparticles. In order to gain further insight in the host-guest interactions, ab initio molecular dynamics (AIMD) calculations were performed on adsorbed taxol within periodic structure of UiO-67* containing one linker defect. Taxol adsorption in UiO-66* wasn't studied, because there was no enough space to incorporate taxol,

This journal is © The Royal Society of Chemistry 20xx

View Article Online
DOI: 10.1039/C7QI00645D

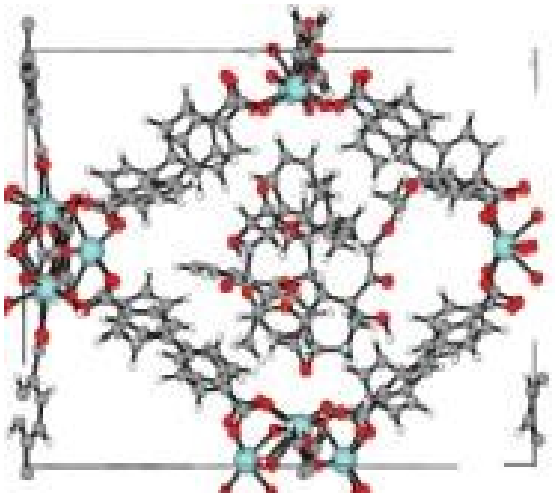

Fig. 7 Visualization of the MD simulation snapshot (t=5 ps) of taxol in UiO-67*. Reprinted from Biocompatible Zr-based nanoscale MOFs coated with modified poly(ε-caprolactone) as anticancer drug carriers, 509/1-2, M. Filippousi, S. Turner, K. Leus, P. I. Siafaka, E. D. Tseligka, M. Vandichel, S. G. Nanaki, I. S. Vizirianakis, D. N. Bikiaris, P. Van Der Voort and G. Van Tendeloo, Int J Pharm., 208-18, Copyright (2016), with permission from Elsevier.

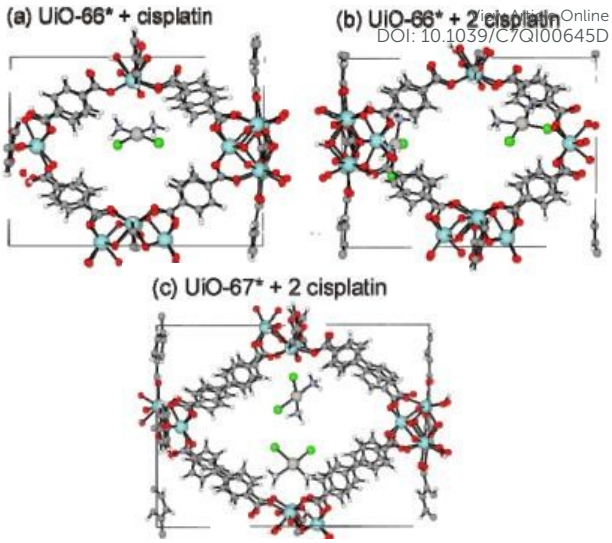

Fig. 8 Visualization of the MD simulation snapshots (t=5 ps) of cisplatin in UiO-66* and UiO-67*. Reprinted from Biocompatible Zr-based nanoscale MOFs coated with modified poly(ε-caprolactone) as anticancer drug carriers, 509/1-2, M. Filippousi, S. Turner, K. Leus, P. I. Siafaka, E. D. Tseligka, M. Vandichel, S. G. Nanaki, I. S. Vizirianakis, D. N. Bikiaris, P. Van Der Voort and G. Van Tendeloo, Int J Pharm., 208-18, Copyright (2016), with permission from Elsevier.

without the presence of at least inorganic secondary building units (SBUs) defects. Fig. 7 depicts the simulation snapshot obtained after 5 ps of the performed MD run within the NVT ensemble (P=1bar, T=298K), from which the favorable adsorption sites of taxol molecule can be visualized. Specifically, taxol fills in the entire pore of UiO-67*, exhibiting limited mobility of the drug molecule in the MOF's pore and consequently prolongs the drug release rate.

From Filippousi *et* al. study on taxol and cisplatin delivery in UiO-66 and UiO-67, we can conclude that MD simulations are able to shed light on the diffusion properties and adsorption sites of the drug molecules within MOFs' pores. This study revealed that these Zr-based nMOFs are potent drug carriers for important anti-cancer agents' delivery, due to both their porous and crystalline structures that are able to deliver the drugs in a controlled manner, and the extra biocompatibility of their polymeric coatings.

3.4.1.3 Cisplatin

Filippousi *et* al.,[80] studied the potential use of two biocompatible and biodegradable nMOFs, UiO-66 and UiO-67, as promising anti-cancer platforms for the cisplatin delivery. Hydrophilic cisplatin was adsorbed in both MOF structures and the experimental loading was around 48 mg/g in UiO-66 and 10 mg/g in UiO-67. In order to gain further insight in the drug-MOF interactions, AIMD calculations were performed on adsorbed cisplatin within periodic structures of UiO-66* and UiO-67*containing one linker defect. Fig. 8 depicts the simulation snapshots obtained after 5 ps of the executed MD run within the NVT ensemble (P=1bar, T=298K), from which the favorable adsorption sites of cisplatin molecule can be recognized. Specifically, cisplatin molecules are in close contact with the binding site Zr-O-Zr of the metal clusters of both frameworks (Fig. 8a and c). As is depicted in Fig 8c, UiO-67* the enough void space caused by incorporation of one linker defect, makes it feasible for two drug molecules to interact with two opposite metal clusters, while in the case of UiO-66* only one cisplatin molecule binds to the Zr-O-Zr site (Fig. 8b).

3.4.1.4 Bu

Chalati *et* al.,[69] performed periodic DFT calculations to investigate the most favorable conformations and binding sites of Bu into MIL-53(Fe) and the functionalized MIL-53(Fe)-NH_2. In the case of MIL-53(Fe), the binding energy with Bu was calculated at 16.64 kcal/mol and the most energetically favorable configuration was obtained by the PW91/DNP method.[81,82] The high binding energy can be attributed to the formation of hydrogen bonds between Bu and the host MOF. Specifically, an oxygen atom of the sulfonate groups of Bu strongly interacts with the μ2-OH hydroxyl group of the framework ($O_{(sulfonate)}$-$H_{(\mu2\text{-}OH)}$ = 1.68 Å). The complex is further stabilized by additional vdW and C-H/π interactions between both sulfonate and methyl groups of the Bu molecule and the organic linker of MIL-53(Fe).

In the case of the modified MIL-53(Fe)-NH_2, the binding energy with Bu was calculated at 17.78 kcal/mol and the most energetically favorable configuration was obtained with the same method. The enhanced binding energy is due to the existence of an additional interaction between the oxygen atom of the sulfonate group of Bu

and the -NH_2 group of the modified structure with a characteristic distance of 2.35 Å.

This study revealed that the incorporation of an amino group in MIL-53 structure introduced an additional binding site with Bu, improving the binding energy for MIL-53-NH_2 about 8% over the unmodified one. Such an enhancement of the MOF-drug interactions could lead to a more slow and controlled release, reducing the severe effects of the conventional drug.

Ma *et* al.,[83] studied a non-toxic hydrostable nitryl/methyl-functionalized Zn-MOF for Bu delivery, with chemical formulae $[Zn(NO_2–BDC)\ (dmbpy)_{0.5}]\cdot(C_2H_6O)\cdot(H_2O)$ (1) (NO_2–BDC = 5-nitroisophthalate, dmbpy =2,2′-dimethyl-4,4′-bipyridine, C_2H_6O = ethanol). Experimental studies exhibited a very porous framework with high Bu payloads of around 17.2 wt % and a sustained release of the drug with no initial burst effect. In particular, the delivery of Bu achieved within 36h, and 100% of the loaded drug was released in PBS. The hydrogen-bonding and C−H/π stacking interactions between the drug molecules and the host MOF, might be the driving force for the slow release of the drug, showing consistence with the molecular simulation results (Fig. 9). Periodic DFT simulations with the method PW91 were performed, to gain further insight into the drug behavior in the MOF structure. Fig. 9 depicts the optimized geometry of Bu with respect to 1, in which the nitryl and methyl groups of the framework interact with the drug molecules. In addition, GCMC calculations were performed and the Q_{st} of Bu in 1 at infinitive dilution at 298 K was calculated at 40.14 kcal/mol, indicating MOF strong Bu adsorption capacity and therefore prolonged drug release.

From this study, we can conclude that the decoration of the MOF framework with hydrophobic nitryl/methyl groups, enhanced the MOF stability in water, making it a very potent non-toxic carrier for anti-cancer drug delivery. Moreover, the high adsorption capacity and the sustained drug release characteristics of the framework, reinforce this potency.

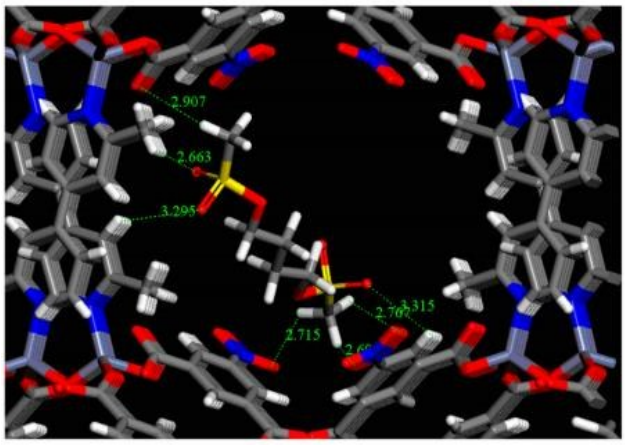

Fig. 9 Optimized geometry of Bu with respect to 1, as obtained from periodic DFT calculations. Reprinted with permission from {D. -Y. Ma, Z. Li, J. -X. Xiao, R. Deng, P. -F. Lin, R. -Q. Chen, Y. -Q. Liang, H. -F. Guo, B. Liu, and J. -Q. Liu, *Inorg. Chem.*, 2015, **54**(14), 6719–6726}. Copyright {2015} American Chemical Society.

3.4.1.5 DOX

Vasconcelos *et* al.,[71] studied the loading and release of the anti-cancer drug, DOX, from ZIF-8. The experimental results revealed a DOX loading into ZIF-8 of about 49 wt% and a very slow release rate which lasts for 30 days. Molecular docking calculations were performed to investigate the drug-matrix interactions and expose the favourable conformations of DOX into ZIF-8 structure. The calculations showed that DOX binds mainly to the surface rather than into the pores of the framework, supporting the experimental results. Specifically, DOX interacts with the Zn^{2+} ions on the ZIF-8 surface *via* quinone and phenolic oxygens of the anthracycline part of the drug.

From this study, we can conclude that ZIF-8 is a very rigid material with high-load and progressive release properties, making it a very promising carrier for anti-cancer drug delivery.

3.4.1.6 Imatinib

Qi *et* al.,[84] reported a study of MIL-101 as a potent adsorbent in the extraction of analyte molecules in plasma samples. Molecular docking calculations were carried out to investigate the molecular interactions and binding energies between host MOFs and guest molecules, gaining further insight into the adsorption mechanism. The most favorable configurations of MIL-101(Cr) and MIL-100(Fe) with imatinib and Sulfamethoxazole (internal standard, IS), were identified (Fig. 10). Specifically, in the case of host MOFs towards

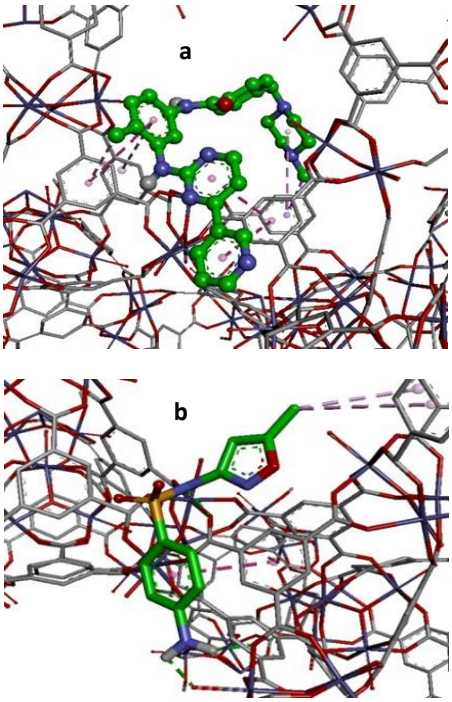

Fig. 10 Favorable configurations between MIL-100(Fe) and imatinib (a) and I (b). Reprinted from The metal-organic framework MIL-101(Cr) as efficier adsorbent in a vortex-assisted dispersive solid-phase extraction of imatini mesylate in rat plasma coupled with ultra-performance liqui chromatography/mass spectrometry: Application to a pharmacokinetic stud 1449, C. Qi, Q. Cai, P. Zhao, X. Jia, N. Lu, L. He and X. Hou, J Chromatogr A., 3(8, Copyright 2016), with permission from Elsevier.

This journal is © The Royal Society of Chemistry 20xx

imatinib (Fig. 10a), the open metal sites in MOFs interact with the amide group in imatinib structure and the complex is further stabilized by i) additional hydrogen bonds between the carboxyl group in MOFs and the amino group in imatinib, ii) π-π interactions and hydrophobic effects between the phenyl rings of MOFs and imatinib and iii) vdW interactions between the MOFs and the imatinib. All these interactions are the driving force for the efficient adsorption of imatinib on the surface of MIL-101(Cr) or MIL-100(Fe). The binding energy of MIL-101(Cr) towards imatinib and IS was calculated at 9.90 and 7.89 kcal/mol respectively, while in the case of MIL-100(Fe) towards imatinib and IS was calculated at 9.17 and 6.46 kcal/mol respectively. The stronger interaction between MIL-101(Cr) and the analyte molecules was achieved because MIL-101(Cr) has a higher surface area and pore aperture than MIL-100(Fe), and thus imatinib would be adsorbed into MIL-101(Cr) more easily.

The simulations results were in good agreement with the experiments, revealing the MIL-101(Cr) as the suitable sorbent in analyte enrichment from complex biosamples.

3.4.1.7 Tamoxifen (TAM)

Koukaras *et* al.,[85] presented a first-principles study on anti-cancer drug delivery of TAM through IRMOF-14 and IRMOF-16 pores. In particular, calculations at MP2[86,87] and DFT levels of theory have been performed to evaluate the nature of MOF-drug interactions and the favorable arrangement of TAM around host MOFs. The organic linker of both MOFs was modified by inserting a hydroxyl group in order to introduce a key binding site of TAM with the functionalized OH-IRMOFs and to enhance the drug/MOF interaction. The initial geometries of the complexes were adopted with the PBE/TZVP[88] method, and then were used as starting geometries for further optimization with the very precise MP2/TZVP method. In the case of IRMOF-14 the binding energy with TAM was calculated at 16.16 kcal/mol and can be attributed to the interaction between i) the nitrogen atom of TAM and the hydrogen atom of the hydroxyl group of IRMOF-14 organic linker, named as hPDC, ($N_{TAM}\cdots HO_{hPDC}$=1.8 Å) and ii) the oxygen atom of TAM and the hydrogen atom of the hydroxyl group of hPDC ($O_{TAM}\cdots HO_{hPDC}$=2.8 Å). In the case of IRMOF-16 the binding energy with TAM was calculated at 18.32 kcal/mol and can be attributed to the interaction between the nitrogen atom of TAM and the hydrogen atom of the hydroxyl group of IRMOF-16 organic linker, named as hTPDC ($N_{TAM}\cdots HO_{hTPDC}$=1.94 Å). The modified IRMOF-16 exhibited enhanced binding energy with TAM, due to the existence of hydrogen bonding interactions coupled with weaker π-π interactions that contribute significantly to overall binding.

This study revealed that the incorporation of a hydroxyl group in IRMOFs' structures introduced an additional binding site with TAM, improving the binding energy for IRMOF-16 more than 50% over the unmodified one. The maximum binding energies of 16.16 kcal/mol for IRMOF-14 and 18.32 kcal/mol for IRMOF-16 are suitable for drug adsorption and delivery with a slow release (binding without overbinding) as reported by Babarao *et* al.[32]

3.4.1.8 Gemcitabine (GEM)

In our work,[89] an OH-functionalization strategy in MOFs for drug delivery was reported. Firstly, we strategically modified the organic linker of IRMOF-16 (named as TPDC) by inserting a hydroxyl group, in order to introduce an additional binding site with GEM. Then, DFT calculations were carried out to identify the most favorable conformations and adsorption sites between MOF/drug and subsequently the loading capacity of the frameworks was calculated using GCMC calculations. In the case of the modified OH-IRMOF-16 molecular fragment, the binding energy with GEM was calculated at 22.6 kcal/mol and the energetically favorable configuration is depicted in Fig. 11 as was obtained by the RI[90]-PBE-D3/def2-TZVP method. The high binding energy can be attributed to the formation of hydrogen bonds between GEM and the host MOF. Specifically, a hydroxyl group of GEM strongly interacts with the hydroxyl group of OH-TPDC linker (OH_{GEM}-OH_{TPDC} = 2.5 Å) and the complex is further stabilized by additional hydrogen bonds between i) the nitrogen atom of GEM and the hydroxyl group of OH-TPDC (OH_{TPDC}-N_{GEM} = 2.2 Å) and ii) the amine group of GEM and the hydroxyl group of OH-TPDC (H_{NH2}-OH_{TPDC} = 2 Å). The binding energy of GEM with the unmodified molecular model of IRMOF-16 was calculated at 15.8 kcal/mol.

Subsequently, the maximum adsorption capacity of GEM in the modified OH-IRMOF-16 and the unmodified framework was calculated performing GCMC calculations for a large fugacity range i.e. 10^{-15}- 10^{5} Pa and at 310 K. The saturated loading was determined to be 4343 and 4749 mg of GEM per g of OH-functionalized-IRMOF-16 and the unmodified one respectively, revealing a slight increased uptake for the unmodified framework. The increased adsorption capacity of IRMOF-16 has to do with the larger free volume of the unmodified structure, as it has been observed in similar studies.[31] Release rate profiles were also obtained from GCMC calculations, indicating a slower drug release rate in the case of the modified structure, due to the enhanced drug/MOF interaction as was also confirmed from the DFT calculations for the OH-IRMOF-16 framework.

In this study, we proposed a strategy of introducing an –OH group into the MOF structure, providing an additional binding site

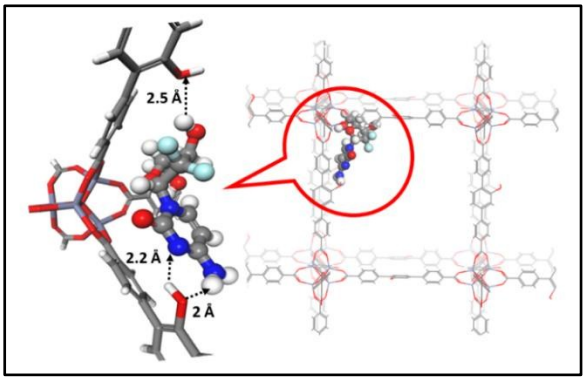

Fig. 11 The most stable configuration of OH-IRMOF-16 molecular fragment with GEM as derived from DFT calculations. Reprinted from OH-functionalization strategy in Metal-Organic Frameworks for drug delivery, 685, M. Kotzabasaki, E. Tylianakis, E. Klontzas and G. E. Froudakis, Chem. Phys. Lett., 114-118. Copyright (2017), with permission from Elsevier.

View Article Online
DOI: 10.1039/C7QI00645D

ARTICLE

with GEM and thus improving the binding energy about 40% compared to the unmodified structure. High storage performance (> 4000 mg/g) for both MOFs was achieved, outperforming more than 10 times other conventional drug delivery systems (Mesoporous Silica Nanoparticle 400 mg GEM/g).[91] The GEM uptake is a function of the free volume of the structures rather than of the MOF functionalization, while a slower drug release rate is more pronounced in the case of the modified OH-IRMOF-16.

In another study,[56] we performed multiscale simulations to investigate GEM adsorption and diffusion in IRMOF-74-III and in the modified OH-IRMOF-74-III. In the case of OH-IRMOF-74-III molecular fragment, the binding energy with GEM was calculated at 33.8 kcal/mol and the energetically favorable configuration is depicted in Fig. 12, as was obtained by the RI-PBE-D3/def2-TZVP method. The high binding energy can be attributed to the formation of hydrogen bonds between GEM and the host MOF. **I**n the case of OH-IRMOF-74- III (Fig. 12a), the carbonyl group of GEM strongly interacts with the hydroxyl group of the OH-linker ($OH_{MOF}\cdots O_{GEM}$, 2.2 Å). The complex is further stabilized by additional hydrogen bonds between i) the amine group of GEM and the oxygen atom of MOF ($H_{NH2}\cdots O_{MOF}$, 2.1 Å), ii) the hydroxyl group of GEM and the water molecule coordinated to MOF ($OH_{H20}\cdots OH_{GEM}$, 1.9 Å), and iii) the hydroxymethyl group of GEM and the oxygen atom coordinated to MOF ($OH_{GEM}\cdots O_{MOF}$, 1.8 Å). In the case of the unmodified molecular fragment of IRMOF-74-III, the binding energy with GEM was calculated at 30.9 kcal/mol with the same method and the complex's favorable conformation is depicted in Fig. 12b. The figure indicates that the amine group of GEM interacts with the oxygen atom of MOF ($H_{NH2}\cdots O_{MOF}$, 2.1 Å) and the complex is further stabilized by additional hydrogen bonds between i) the hydroxymethyl oxygen of GEM and the MOF coordinated water ($OH_{H20}\cdots OH_{GEM}$, 1.8 Å), and ii) the hydroxymethyl hydrogen of GEM and the oxygen atom of the MOF ($OH_{GEM}\cdots O_{MOF}$, 1.7 Å).

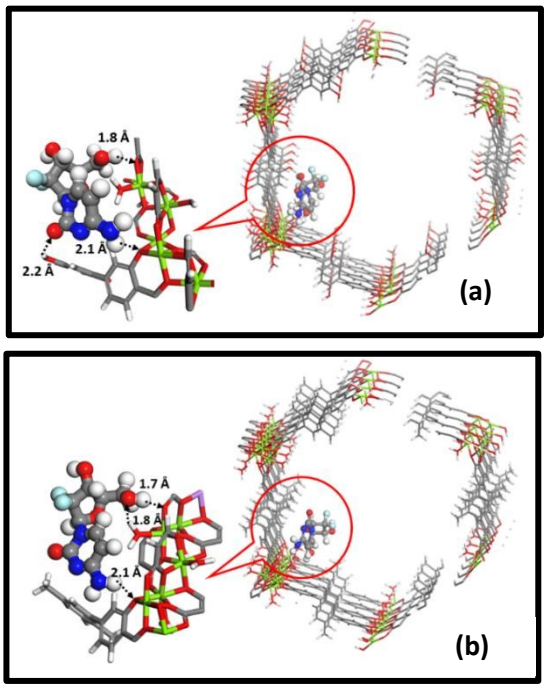

Fig. 12 Optimized geometries of GEM with respect to (a) the OH-IRMOF-74-III, and (b) the IRMOF-74-III molecular fragments as those derived from DFT calculations. Reproduced ("Adapted") from (Ref 56) with permission of The Royal Society of Chemistry.

Subsequently, the maximum adsorption capacity of GEM in IRMOF-74-III and OH-IRMOF-74-III was calculated performing GCMC calculations for a large fugacity range i.e. 10^{-15}- 10^{5} Pa and at 310 K. The simulation results revealed that the saturated loading for both IRMOF systems is the same. The saturated loading was determined to be 1130 mg of drug molecule per g of the framework. Given that both structures exhibit the same large pore aperture (~25 Å) the calculation of the same uptake of GEM in both structures is related to the fact that the maximum drug loading is a function of the free volume rather than of the functionalization of the framework, as it has been observed in similar studies.[31,89]

MD simulations in the NVT ensemble at 310 K were carried out to gain insight the diffusion of 32, 63 and 95 wt% GEM molecules in the pores of host MOFs. The simulations revealed that Diffusion coefficient (D) values of GEM inside each MOF decrease with increasing loading. In the case of OH-IRMOF-74-III the D values are slightly increased compared to the unmodified framework. The density profiles of GEM molecules in the pores of host MOFs indicated an increased tendency for formation of drug aggregations in IRMOF-74-III, explaining the lower mobility of GEM in the pores of the unmodified material.

In this work, QM results indicated that the interaction energy of GEM with both MOFs is similar. GCMC results revealed high GEM adsorption capacity for both MOFs systems with a maximum drug loading that outperforms other conventional drug delivery systems such as a proposed Lipid-Coated Mesoporous Silica Nanoparticle Platform for the GEM delivery (400 mg GEM/g)[91] and has a similar loading to liposome systems (1500 mg GEM/g lipid).[92] Lastly, the mobility of GEM was of the same magnitude inside both MOFs pores. This multiscale approach revealed that IRMOF-74-III and OH-IRMOF-74-III are equally auspicious nanocarriers for storage of GEM.

From both of our studies, we can conclude that following the strategic modification of the selected MOFs, highly desirable multipoint, noncovalent, binding with the studied drug and thus a slow drug release profile was attained. Interaction energies of about 20-30 kcal/mol are suitable for drug's adsorption and delivery with slow release. High drug loading capacity for IRMOF structures imply

This journal is © The Royal Society of Chemistry 20xx

View Article Online
DOI: 10.1039/C7QI00645D

ARTICLE

MOF(s)	Drugs	Method(s)	Ref.
$(Sm_3(L1)_2(HCOO)_2(DMF)_2(H_2O)]\cdot 2DMF\cdot 18H_2O$	5-FU	GCMC	75
$[(Cu_2(L2)(H_2O)_2]\cdot 2.22DMA$	5-FU	GCMC	75
$[(Zn_2(L1)(DMA)]\cdot 1.75DMA$	5-FU	GCMC	75
$[Zn_3(\mu_3\text{-}O)(BTC)_2(H_3O)]_n$	5-FU	GCMC	76
$\{[Zn_3(\mu_3\text{-}O)(BTC)_2(DMF)]\cdot 2NH_2(CH_3)_2\cdot 4H2O\}_n$	5-FU	GCMC	76
$\{[Zn_2(fer)_2]\}_n$	5-FU	GCMC	77
$[Cu(L)(4,4'\text{-bipy})(H2O)]_n\cdot 1.5_nCH_3CN$	5-FU	Molecular docking	78
$[Cu(L)(4,4'\text{-bipy})(H2O)]_n\cdot 4_nH_2O$	5-FU	Molecular docking	78
$Co_2(L)(4,4'\text{-Bipy})_2] \cdot CH_3CN\}_n$	5-FU	AM1	79
UiO-66	Taxol	AIMD	80
UiO-67	Taxol	AIMD	80
UiO-66	Cisplatin	AIMD	80
UiO-67	Cisplatin	AIMD	80
MIL-53(Fe)	Bu	DFT	69
MIL-53(Fe)-NH2	Bu	DFT	69
$[Zn(NO_2\text{–}BDC)(dmbpy)_{0.5}]\cdot(C_2H_6O)\cdot(H_2O)$	Bu	DFT, GCMC	83
ZIF-8	DOX	Molecular Docking	71
MIL-101(Cr)	Imatinib, SI	Molecular Docking	84
MIL-101(Fe)	Imatinib, SI	Molecular Docking	84
IRMOF-14	TAM	DFT, MP2	85
IRMOF-16	TAM	DFT, MP2	85
IRMOF-16	GEM	DFT, GCMC	89
IRMOF-74	GEM	DFT, GCMC, MD	56

Table 5 Summary of molecular simulations of anti-cancer drug delivery in MOFs.

that a limited amount of material is required for administration of high doses. Besides favorable drug-host interactions, a crucial factor in drug delivery is tunable loadings. The correlation of GEM uptake with the free volume of studied MOFs rather than the functionalization of the MOF surface indicates that desired loading can be achieved by tuning the pore size with bulky functional groups**.** Multiscale modelling that comprises DFT, GCMC and MD simulations that was applied to the study of drug-MOF energetics & dynamics, demonstrates that this approach should be generalized to the study of nanocarrier-drug interactions and drug diffusion, prior experimental investigation.

3.4.1.9 Summary

Above, in Table 5, we briefly present the molecular simulations of anti-cancer drug delivery in MOFs that have been reported in this review.

The simulations revealed that the drug molecules can be incorporated in high loadings within the MOFs and can be released slowly, presenting a much-improved therapeutic profile. This provides more and more impetus on using appropriate MOFs to control anti-cancer drug delivery.

Conclusions and remarks

This article has particularly described the virtues of using molecular simulations to study anti-cancer drug delivery in MOFs. Advantages are multifold: I) by performing DFT calculations or analysing the trajectories obtained from classical simulations, the favorable adsorption sites of the chemotherapeutics in the MOFs' pores have been identified, II) by performing GCMC or molecular dynamics simulations, the maximum drug loading capacity and the diffusion coefficient of the drug molecules in each material has also been estimated and III) by combining data from multiple techniques a clear molecular-level understanding for anti-cancer storage and release mechanisms has been achieved. Table 5 in this review summarizes a list of MOFs that have been screened as potential drug carriers using molecular simulations.

From the MOFs' molecular screening, many conclusions can be drawn. The drug loading capacity of each MOF structure, is related to its pore characteristics and the nature of host-guest interactions. Regarding the porosity of the host material, the drug loading capacity increases as a function of the void space and no direct relation as a function of the surface area or the pore geometry has been reported so far. With regard to the surface chemistry of the pore, the effect of functionalization is no so significant for the maximum drug loading capacity of the material, but it may alter the density profiles of the drug molecules inside the pores.

Comparing the theoretical with the experimental results, we have concluded that the theoretical methods can accurately reproduce the drug loading values in MOFs within the same order of magnitude of the experimental values, while offering a microscopic, structure-based perspective of the drug adsorption mechanism in porous materials. Regarding the drug release mechanism, simulations revealed that the strong interactions between MOF-drug complexes decrease the mobility of the drug in host MOF, and hence are responsible for the prolonged release rate. The release time is correlated to the diffusion of the drug within the MOFs pores as shown using experimentally-derived kinetic models for the drug-MOF release.

This review underscores that MOFs having high storage performance and sustained drug release properties could offer a great and highly tunable drug delivery solution to the challenge of how to improve the *in vivo* characteristics and overall efficacy of many important anti-cancer drugs, bringing to light a new hope for cancer treatment. A lot of aspects should be addressed before the practical use of MOFs in cancer therapy. Work on the near future should be concentrated more on the biocompatibility, colloidal stability, biodistribution and accumulation, including cellular transit, degradation, excretion, physiological barrier penetration and chronic toxicity of MOFs' structures. So, further experimental studies of the pharmacokinetics and efficiency of anti-cancer drug-containing MOFs in the living organisms, should be the next vital steps to evaluate their real performance in medical research.

View Article Online
DOI: 10.1039/C7QI00645D

Acknowledgements

This work was supported by the Program "Research Projects for Excellence IKY/Siemens, in the framework of the Hellenic Republic – Siemens Settlement Agreement".

Notes and references

1 National Institutes of Health (US); Biological Sciences Curriculum Study. NIH Curriculum Supplement Series [Internet]. Bethesda (MD): National Institutes of Health (US); 2007. Understanding Cancer. Available from: https://www.ncbi.nlm.nih.gov/books/NBK20362/.
2 The website of the National Cancer Institute available from: https://www.cancer.gov.
3 R. L. Siegel, K. D. Miller and A. Jemal, *CA CANCER J CLIN*, 2017, **67**(1), 7-30.
4 C. M. O'Connor and J. U. Adams, Essentials of Cell Biology. Cambridge, MA: NPG Education, 2010.
5 V. T. DeVita and E. Chu, *Cancer Res*, 2008, **68**(21), 8643–53.
6 D. S. Shewach and R. D. Kuchta, *Chem Rev.*, 2009, **109**(7), 2859-61.
7 The website of the Canadian Cancer Society available from: www.cancer.ca.
8 Y. H. Bae, R. J. Mrsny and K. Park, Cancer Targeted Drug Delivery: An Elusive Dream. New York, Springer Science & Business Media, 2013.
9 X. Wang, S. Li, Y. Shi, X. Chuan, J. Li, T. Zhong, H. Zhang, W. Dai, B. He and Q. Zhang, *J Control Release*, 2014, **193**, 139-153.
10 J. L. Markman, A. Rekechenetskiy, E. Holler and J. Y. Ljubimova, *Adv Drug Deliv Rev*, 2013, **65**, 1866-1879.
11 X. Wang, L. Yang, Z. Chen and D. M. Shin, *CA Cancer J Clin*, 2008, **58**, 97-110.
12 M. F. Tang, L. Lei, S. R. Guo and W. L. Huang, *Chin J Cancer*, 2010, **29** (9), 775-780.
13 A. Patri, I. Majoros and J. Baker, *Curr. Opin. Chem. Biol.*, 2002, **6**(4), 466-471.
14 S. Freiberg and X. X. Zhu, *Int. J. Pharm.*, 2004, **282**, 1–18.
15 A. Rivera and T. Farías, *Microporous Mesoporous Mater.*, 2005, **80**, 337–346.
16 M. Vallet-Regí, A. Rámila, R. P del Real and J. Perez-Pariente, *Chem. Mater.*, 2001, **13**, 308–311.
17 F. Alexis, E. M. Pridgen, R. Langer, and O. C. Farokhzad, *Handb Exp Pharmacol.*, 2010, **197**, 55-86.
18 J. Agnihotri, S. Saraf and A. Khale, *Int J Pharm Sci Rev Res*, 2011, **8**(2), 117-123.
19 V. P. Torchilin, *Handb Exp Pharmacol.*, 2010, **197**, 3-53.
20 P. Siafaka, N. Üstündağ Okur, E. Karavas, and D. Bikiaris, *Int. J. Mol. Sci.*, 2016, **17**, 1440.
21 P. Siafaka, M. Betsiou, A. Tsolou, E. Angelou, B. Agianian, M. Koffa, S. Chaitidou, E. Karavas, K. Avgoustakis and D. Bikiaris, *J Mater Sci: Mater Med*, 2015, **26**, 275.
22 V. Karavelidis, D. Bikiaris and K. Avgoustakis, *J Pharm Pharmacol*, 2015, **67**, 215–230.
23 S. Kyriakopoulou, G. Mattheolabakis, S. Papadimitriou, E. Karavas, D. Bikiaris and K. Avgoustakis, *Curr Nanosci*, 2011, **7**(4), 503-509(7).
24 J. L. C Rowsell and O. M. Yaghi, *Mic. Mes. Mater.*, 2004, **73**, 3-14.
25 S. Keskin and S. Kızılel, *Indus. & Engin. Chem. Res.*, 2011, **50** (4), 1799-1812.
26 P. Horcajada, C. Serre, M. Vallet-Reg, M. Sebban, F. Taulelle and G. Ferey, *Angew. Chem. Int.*, 2006, **45**, 5974–5978.

This journal is © The Royal Society of Chemistry 20xx

View Article Online
DOI: 10.1039/C7QI00649D

27 R. C. Huxford, J. D. Rocca and W. Lin, *Curr. Opin. Chem. Bio.*, 2010, **14** (2), 262–268.
28 P. Horcajada, C. Serre, G. Maurin, N. A. Ramsahye, F. Balas, M. Vallet-Regí, M. Sebban, F. Taulelle and G. Férey, *J. Am. Chem. Soc.*, 2008, **130**, 6774–6780.
29 P. Horcajada, R. Gref, T. Baati, P. K. Allan, G. Maurin, P. Couvreur, G. Ferey, R. E. Morris and C. Serre, *Chem. Rev.*, 2012, **112**, 1232-1268.
30 A. C. McKinlay, R. E. Morris, P. Horcajada, G. Férey, R. Gref, P. Couvreur and C. Serre, *Angew. Chem. Int. Ed.*, 2010, **49**(36), 6260-6266.
31 I. Erucar and S. Keskin, *Ind. Eng. Chem. Res.*, 2016, **55**(7), 1929-1939.
32 R. Babarao and J. Jiang, *J. Phys. Chem. C*, 2009, **113**, 18287–18291.
33 M. Bernini, D. Fairen-Jimenez, M. Pasinetti, A. Ramirez-Pastor .and R. Snurr, *J. Mater. Chem. B*, 2014, **2**(7), 766-774.
34 D. Fatouros, D. Douroumis, V. Nikolakis, S. Ntais, A. Moschovi, V. Trivedi, B. Khima, M. Roldo, H. Nazar and P. Cox, *J. Mat. Chem.*, 2011, **21**(21), 7789.
35 P. W. Atkins and R. S. Friedman, Molecular Quantum Mechanics. New York, Oxford University Press, 2011.
36 D. Frenkel and B. Smit, Understanding Molecular Simulation: From Algorithms to Applications (2nd ed.). Florida, Academic Press, 2002.
37 E. Tylianakis, E. Klontzas, G. E. Froudakis, *Nanoscale*, 2011, **3**(3), 856-869.
38 S. O. Odoh, C. J. Cramer, D. G. Truhlar, and L. Gagliardi, *Chem. Rev.*, 2015, **115**(12), 6051–6111.
39 J. Jiang, *Mol Sim*, 2014, **40**(7-9), 516-536.
40 F. X. Coudert and A. H. Fuchs, *Coord. Chem. Rev.*, 2016, **307**(2), 211-236.
41 J. P. Perdew, K. Burke and M. Ernzerhof, *Phys. Rev. Lett.*, 1996, **77**, 3865−3868.
42 S. Grimme, J. Antony, S. Ehrlick, S. Krieg, *J. Chem. Phys.*, 2010, **132,** 154104.
43 K. I. Ramachandran, G. Deepa and K. Namboori, Computational Chemistry and Molecular Modeling Principles and Applications, Springer Science & Business Media, 2008.
44 X.-Y. Meng, H.-X. Zhang, M. Mezei and M. Cui, *Curr Comput Aided Drug Des*, 2011, **7**(2), 146–157.
45 M. O. Rodrigues, M. V. de Paula, K. A. Wanderley, I. B. Vasconcelos, S. Alves and T. A. Soares, *Int. J. Quantum Chem.*, 2012, **112**, 3346–3355.
46 A. Hinchliffe, Molecular Modelling for Beginners (2nd ed.), John Wiley & Sons Ltd, 2008.
47 A. K. Rappe, C. J. Casewit, K. S. Colwell, W. A. Goddard and W. M. Skiff, *J. Am. Chem. Soc.*, 1992, **114**(25), 10024–10035.
48 S. L. Mayo, B. D. Olafson and W. A. Goddard, *J. Phys. Chem.*, 1990, **94**(26), 8897–8909.
49 W. D. Cornell, P. Cieplak, C. I. Bayly, I. R. Gould, K. M. Merz, D. M. Ferguson, D. C. Spellmeyer, T. Fox, J. W. Caldwell and P. A. Kollman*, J. Am. Chem. Soc.*, 1995, **117**, 5179–5197.
50 D. Y. Peng and D. B. Robinson, *Ind. Eng. Chem. Fundam.*, 1976, **15**, 59–64.
51 B. Widom, *J. Chem. Phys.*, 1963, **39**(11), 2808-2812.
52 A. R. Leach, Molecular Modelling: Principles and Applications (2nd ed.), Pearson Education, 2001.
53 J. E. Lennard-Jones, *Proc. R. Soc. Lond. A*, 1924, **106**(738), 463–477.
54 R. A. Buckingham, *Proc Math Phys Eng Sci*, 1938, **168**(933), 264–283.
55 M. J. Field, A Practical Introduction to the Simulation of Molecular Systems (2nd ed.), Cambridge University Press, 2007.
56 M. Kotzabasaki, I. Galdadas, E. Tylianakis, E. Klontzas, Z. Cournia and G. E. Froudakis, *J. Mater. Chem. B*, 2017, **5**, 3277-3282.
57 S. R. Batten, N. R. Champness, X.-M. Chen, J. Garcia-Martinez, S. Kitagawa, L. Öhrström, M. O'Keeffe, M. P. Suh and J. Reedijk, *Pure Appl. Chem.*, 2013, **85**(8), 1715–1724.
58 M. Kondo, T. Yoshitomi, H. Matsuzaka, S. Kitagawa and K. Seki, Angew. *Chem. Int. Ed.*, 1997, **36**, 1725–1727.
59 S. Horike, S. Shimomura and S. Kitagawa, *Nat Chem*, 2009, **1**, 695 – 704.
60 H. Li, M. Eddaoudi, M. O'Keeffe and O. M. Yaghi, *Nature*, 1999, **402**, 276-279.
61 A. Dhakshinamoorthy, M. Alvaroa and H. Garcia, *Chem. Commun*., 2012, **48**, 11275-11288.
62 C. Tamames-Tabar, A. García-Márquez, M. J. Blanco-Prieto, C. Serre and P. Horcajada, Bio- and Bioinspired Nanomaterials, Wiley-VCH Verlag GmbH & Co. KGaA, 2015.
63 J. An, S. J. Geib and N. L. Rosi, *J. Am. Chem. Soc*., 2009, **131**(24), 8376–8377.
64 C.-Y. Sun, C. Qin, C.-G. Wang, Z.-M. Su, S. Wang, X.-L. Wang, G.-S. Yang, K.-Z. Shao, Y.-Q. Lan and E.-B. Wang, *Adv. Mater*., 2011, **23**(47), 5629–5632.
65 C. He, D. Liu and W. Lin, *Chem. Rev.*, 2015, **115**(19), 11079–11108.
66 W. J. Rieter, K. M. Pott, K. M. L. Taylor and W. Lin, *J. Am. Chem. Soc*., 2008, **130**(35), 11584–11585.
67 K. M. L. Taylor-Pashow, J. D. Rocca, Z. Xie, S. Tran and W. Lin, *J. Am. Chem. Soc*., 2009, **131**(40), 14261–14263.
68 P. Horcajada, T. Chalati, C. Serre, B. Gillet, C. Sebrie, T. Baati, J. F. Eubank, D. Heurtaux, P. Clayette, C. Kreuz, J. S. Chang, Y. K. Hwang, V. Marsaud, P. N. Bories, L. Cynober, S. Gil, G. Férey, P. Couvreur and R. Gref, *Nat Mater.*, 2010, **9**(2), 172-8.
69 T. Chalati, P. Horcajada, P. Couvreur, C. Serre, M. B. Yahia, G. Maurin and R. Gref, *Nanomedicine (Lond)*, 2011, **6**(10), 1683-95.
70 R. Anand, F. Borghi, F. Manoli, I. Manet, V. Agostoni, P. Reschiglian, R. Gref and S. Monti, *J Phys Chem B.,* 2014, **118**(29), 8532-9.
71 I. B. Vasconcelos, T. G. da Silva, G. C. G. Militão, T. A. Soares, N. M. Rodrigues, M. O. Rodrigues, N. B. da Costa, R. O. Freire and S. A. Junior, *RSC Adv.*, 2012,**2**, 9437-9442.
72 C. Adhikari, A. Das and A. Chakraborty, *Mol. Pharmaceutics*, 2015, **12**(9), 3158–3166.
73 W. X. Lin, Q. Hu, J. C. Yu, K. Jiang, Y. Y. Yang, S. C. Xiang, Y. J. Cui, Y. Yang, Z. Y. Wang and G. D. Qian, *ChemPlusChem*, 2016, **81**, 804.
74 W. Cai, C. -C. Chu, G. Liu and Y.-X. J. Wáng, *Small*, 2015, **11**, 4806–4822.
75 J.-Q.Liu, X.-F. Li, C.-Y. Gu, J. C. S. da Silva, A. L. Barros, S. Alves-Jr, B.-H. Li, F. Ren, S. R. Battene and T. A. Soares, *Dalton Trans.*, 2015,**44**, 19370-19382.
76 J. Wang, J. Jin, F. Li, B. Li, J. Liu, J. Jin, C. Wang, Y. Zeng and Y. Wang, *RSC Adv.*, 2015,**5**, 85606-85612.
77 F. Li, B. Li, C. Wang, Y. Zeng, J. Liu, C.-Y. Gu, P. Lue and L. Meid, *RSC Adv.*, 2016,**6**, 47959-47965.
78 J.-Q. Liu, J. Wu, Z.-B. Jia, H.-L. Chen, Q.-L. Li, H. Sakiyama, T. Soares, R. Fei, C. Daiguebonne, O. Guillou and S. W. Ng, *Dalton Trans.*, 2014,**43**, 17265-17273.
79 F. M. Wang, J. Wang, S. Z. Yang, C. Y. Gu, X. R. Wu, J. Q. Liu, H. Sakiyama, J. W. Xu, M. M. Luo and W. C. Liu, *Russ. J. Coord. Chem*., 2017, **43**(2), 133–137.
80 M. Filippousi, S. Turner, K. Leus, P. I. Siafaka, E. D. Tseligka, M. Vandichel, S. G. Nanaki, I. S. Vizirianakis, D. N. Bikiaris, P. Van Der Voort and G. Van Tendeloo, *Int J Pharm.*, 2016, **509(**1-2), 208-18.
81 J. P. Perdew and Y. Wang, *Phys. Rev. B*, 1992, **45**, 13244–13249.
82 W. J. Hehre, R. Ditchfield and J. A. Pople, *J. Chem. Phys.*, 1972, **56**, 2257–2261.

83 D. -T. Ma, Z. Li, J. -X. Xiao, R. Deng, P. -P. Lin, R. -Q. Chen, T. -Q. Liang, H. -F. Guo, B. Liu, and J. -Q. Liu, *Inorg. Chem.*, 2015, **54**(14), 6719–6726.
84 C. Qi, Q. Cai, P. Zhao, X. Jia, N. Lu, L. He and X. Hou, *J Chromatogr A.*, 2016, **1449**, 30-8.
85 E. N. Koukaras, T. Montagnon, P. Trikalitis, D. Bikiaris, A. D. Zdetsis and G. E. Froudakis, *J. Phys. Chem. C*, 2014, **118**(17), 8885–8890.
86 S. Grimme, *J. Chem. Phys.*, 2003, **118**, 9095.
87 R. A. Distasio, *Mol. Phys.*, 2007, **105**, 1073−1083.
88 F. Weigend and R. Ahlrichs, *Phys. Chem. Chem. Phys.*, 2005, **7**, 3297−3305.
89 M. Kotzabasaki, E. Tylianakis, E. Klontzas and G. E. Froudakis, *Chem. Phys. Lett.,* 2017, **685**, 114-118.
90 F. Weigend, M. Häser, H. Patzelt and R. Ahlrichs, *Chem. Phys. Letters.*, 1998, **294**(1-3), 143-152.
91 H. Meng, M. Wang, H. Liu, X. Liu, A. Situ, B. Wu, Z. Ji, C. H. Chang and A. E. Nel, *ACS Nano*, 2015, **9**(4), 3540.
92 C. Celia, N. Malara, R. Terracciano, D. Cosco, D. Paolino, M. Fresta and R. Savino, *Nanomedicine: NBM*, 2008, **4(**2), 155-166.

View Article Online
DOI: 10.1039/C7QI00645D

.

This journal is © The Royal Society of Chemistry 20xx

This journal is © The Royal Society of Chemistry 20xx